Perturbation Analysis of a Planar Periodic Leaky-Wave Antenna Fed by Surface Waves

Samir F. Mahmoud, *Senior Member, IEEE*, Symon K. Podilchak, *Member, IEEE*, Yahia M. M. Antar, *Fellow, IEEE*, and Al P. Freundorfer, *Senior Member, IEEE*

***Abstract*—We consider a printed leaky-wave antenna composed of a grounded substrate topped by a periodic metallic screen or grating. The antenna is fed by the TM_0 surface-wave mode that is launched by an array of slots in the ground plane. The leaky-wave attenuation and phase constants are derived using a simple but accurate field perturbation approach. The radiation power, directivity, and beam patterns are also deduced. Numerical results show that, depending on the screen period and the substrate height, there is an optimum frequency range for maximum radiative power. In addition, calculated results are also in agreement with simulations and measurements for some recently designed and fabricated structures.**

***Index Terms*—Leaky waves (LWs), leaky-wave antenna (LWA), surface waves (SWs), surface-wave launcher (SWL).**

I. Introduction

LEAKY-WAVE antennas (LWAs) have received much interest due to their ease of manufacture and compatibility with other planar devices. They provide conical or directive pencil beams that make them attractive for radar and communication applications. One particular LWA structure, which has been the subject of recent studies [1]–[3], is comprised of a periodic screen or metallic grating placed on a grounded dielectric slab (GDS). Such antennas are typically analyzed using an electric or magnetic dipole source within the substrate.

One simple and practical method for leaky wave (LW) excitation is to launch a bound surface-wave (SW) mode from a slot source embedded within the ground plane of a GDS as depicted in Figs. 1 and 2. Radiation occurs as the guided SW is converted to a LW field along the screened aperture [4]–[6]. An efficient class of such printed surface-wave launcher (SWL) sources has been devised in [7] and further analyzed in [8]. Typically, a high dielectric constant ($\epsilon_r = 10.2$) is used in practice to ensure efficient SW coupling into the dominant TM_0 SW mode of the slab. For unidirectional SW operation, one main slot is fed with a coplanar waveguide transmission line, while parasitic slots act as reflector elements [5]. These SWLs can also be optimized to maximize SW power levels and achieve efficient and guided-wave propagation along the air-dielectric interface [8]. Moreover, in the operating frequency range of these LWAs, GDS thickness and substrate permittivity are typically chosen to support only one TM SW mode.

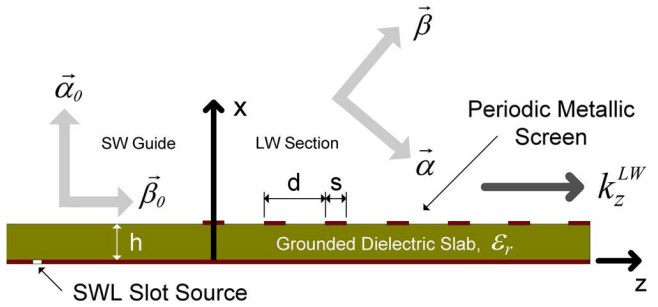

Fig. 1. Planar 1-D LWA under study. The SW region ($x \leq 0$) and the LW section ($x \geq 0$) are illustrated. Radiation of the slot excited TM_0 SW mode occurs by the added metallic grating of periodicity d and strip width s.

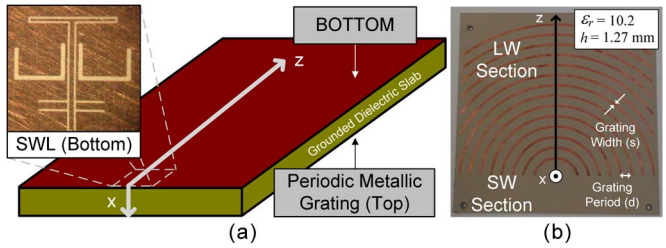

Fig. 2. (a) Illustration of the SW guide and slot feed. (b) Sample LWA structure investigated for verification of the developed analysis. The TM fields directed on such a one-sided radial structure (defined by k_ρ^{LW}) have very similar propagation characteristics (k_z^{LW}) to that of a linear array of metallic strips (Fig. 1), with the same parameters equal to that of the circular gratings [3]. In both cases, propagation is normal to the gratings, as considered in [6] and in the presented perturbation analysis of this letter.

In this letter, we consider the transition from a SW section to a LW section where the bound SW power is gradually transformed into radiative power as energy is leaked away from the planar guiding surface. More specifically, an analysis is completed of a TM_0 SW efficiently launched from the left guide and directed into the right LW region, defined by an infinite linear grating of metallic strips. The phase propagation constant of the incident SW mode, β_0, is then modified to include a small change $\Delta\beta$ and a LW attenuation factor α. In what follows, we derive $\Delta\beta$ and α as well as the radiated power, directivity, and the radiation pattern for the generated LW fields. Results are presented in Figs. 3–5. In addition, the developed analysis is also compared to measurements and simulations of two SWL feed LWA structures (Fig. 6) with

Manuscript received January 22, 2011; revised February 22, 2011; accepted February 26, 2011. Date of publication March 07, 2011; date of current version March 17, 2011.

S. F. Mahmoud is with the Electrical Engineering Department, Kuwait University, Safat 13060, Kuwait (e-mail: samir@eng.kuniv.edu.kw).

S. K. Podilchak, Y. M. M. Antar, and A. P. Freundorfer are with the Electrical Engineering Department, Royal Military College (RMC) of Canada, Kingston, ON K7K 7B4, Canada, and also with the Electrical Engineering Department, Queen's University, Kingston, ON K7L 3N6, Canada (e-mail: skp@ieee.org).

Color versions of one or more of the figures in this letter are available online at http://ieeexplore.ieee.org.

Digital Object Identifier 10.1109/LAWP.2011.2123073

dielectric and strip conductor loss included. Results are in agreement. To the authors' knowledge, this is the first time that such a simple and accurate perturbation analysis has been applied to these SW driven LWA structures.

II. Derivation of the Radiation Fields

Referring to Fig. 1, the substrate thickness h and relative permittivity $\epsilon_{\rm r}$ are chosen to support only one SW mode in the frequency range of interest—the $\rm TM_0$ SW mode. Defining a normalized frequency as F ($= k_0 h\sqrt{\epsilon_{\rm r}-1}$, with $k_0 = \omega\sqrt{\mu_0\epsilon_0}$), single-mode excitation occurs for $F < \pi$. We note here that the SWL does not excite TE modes as long as the incident mode is of type TM and the fields are y-independent, as assumed here, for the 1-D LWA. For a dielectric loss-free structure, the incident and unperturbed SW fields are (assuming an $e^{+j\omega t}$ time variation) $[H_y(x), E_x(x), E_z(x)]e^{-j\beta_0 z}$, where

$$H_y(x) = \begin{cases} H_0\cos(p_s x), & 0 \le x \le h \\ H_0\cos(p_s h)e^{-\alpha_0(x-h)}, & x \ge h \end{cases} \quad (1)$$

with $p_s = \sqrt{\epsilon_r k_0^2 - \beta_0^2}$ and $\alpha_0 = \sqrt{\beta_0^2 - k_0^2}$; $E_x(x)$ and $E_z(x)$ can be obtained from $H_y(x)$ through Maxwell's equations.

Now we turn attention to the leaky waveguide section. The screen is periodic with period "d." Each period contains a thin metal strip of width $s \ll d$, so that the metal strips may be considered as small perturbations on the SW guiding structure. We may then assume that the SW fields remain unperturbed within the dielectric, in the region $0 < x < h$. Namely, the tangential electric field below the interface, $x = h^-$, is equal to $E_z(h)$. However, the same field at $x = h^+$ on the metal strips must vanish. To support such discontinuity, we impose an infinite array of magnetic line sources (with period d) at the positions of the metal strips with a magnetic current density m_y (in [V/m]) given by

$$m_y(x = h^+, z) = \begin{cases} -E_{z0}e^{-j\beta_0 z}, & |z| \le s/2 \\ 0, & s/2 \le |z| \le d/2 \end{cases} \quad (2)$$

where $E_{z0} = (j\alpha_0/\omega\epsilon_0)H_0\cos p_s h$. Note that E_{z0} can be obtained by using the appropriate Maxwell equation ($j\omega\epsilon_0 E_z = \partial H_y/\partial x$) for the region $x \ge h$ from (1) and after the substitution $x = h$.

This infinite array of line sources radiates in the air region in the presence of the unperturbed fields inside the slab. As a periodic function m_y can be expressed in Fourier series form

$$m_y(x = h^+, z) = -E_{z0}\frac{s}{d}e^{-j\beta_0 z} - \sum_{n\neq 0} E_{z0}\frac{s}{d}\mathrm{sinc}\left(\frac{\pi n s}{d}\right)e^{-j\beta_n z} \quad (3)$$

where $\beta_n = \beta_0 + 2\pi n/d$. The summation in (3) runs over all positive and negative integer values of n to account for the excitation of an infinite number of spatial harmonics as m_y is periodic. The $n = 0$ term is intentionally removed from the summation to isolate the perturbation of the fundamental $\rm TM_0$ SW mode above the interface.

Now the z-electric field on the air side of the screen ($x = h^+$) is given by the original E_{z0} field added to the derived perturbation, mainly

$$E_z(x = h^+, z) = E_{z0}\left(1 - \frac{s}{d}\right)e^{-j\beta_0 z} - \sum_{n\neq 0} E_{z0}\frac{s}{d}\mathrm{sinc}\left(\frac{\pi n s}{d}\right)e^{-j\beta_n z}. \quad (4)$$

It is useful to note that as s tends to zero, the metal strips vanish and the $E_z(x = h^+, z)$ field derived in (4) approaches the original E_{z0} field above the interface as expected. Using the wave equation, E_z can also be defined in the air region $x > h$

$$E_z(x, z) = E_{z0}\left(1 - \frac{s}{d}\right)e^{-u_0(x-h)}e^{-j\beta_0 z} - \sum_{n\neq 0} E_{z0}\frac{s}{d}\mathrm{sinc}\left(\frac{\pi n s}{d}\right)e^{-u_n(x-h)}e^{-j\beta_n z} \quad (5)$$

where $u_0 = \sqrt{\beta_0^2 - k_0^2}$ and $u_n = \sqrt{\beta_n^2 - k_0^2}$. The corresponding magnetic field is obtained from Maxwell's equations

$$H_y(x, z) = -j\omega\epsilon_0 E_{z0}\left(1 - \frac{s}{d}\right)e^{-u_0(x-h)}e^{-j\beta_0 z}/u_0 + \sum_{n\neq 0} j\omega\epsilon_0 E_{z0}\frac{s}{d}\mathrm{sinc}\left(\frac{\pi n s}{d}\right)e^{-u_n(x-h)}e^{-j\beta_n z}/u_n. \quad (6)$$

A. Radiated and SW Powers

Now we are in a position to get the power leaked as radiation per unit length "l" along z. Using (2) and (6), we get

$$P_{\rm Rad}/l = -m_y(h, 0)H_y^*(h, 0)s/d = j\omega\epsilon_0|E_{z0}|^2\frac{s}{d}\left[\left(1 - \frac{s}{d}\right)/u_0^* - \frac{s}{d}\sum_{n\neq 0}\mathrm{sinc}\left(\frac{\pi n s}{d}\right)/u_n^*\right]. \quad (7)$$

The summation is over all positive and negative integers of n. It is useful to note that since $\beta_0 > k_0$, u_n is real for all positive values of n. For negative values, u_n can be imaginary whenever $-k_0 < \beta_n < k_0$. The terms that correspond to this condition account for the real part of the radiated power. The other terms account for the reactive component of $P_{\rm Rad}$.

Neglecting any dielectric losses, the SW power flowing along z is purely real and can be derived [8] using (1)

$$P_{\rm SW} = \frac{\eta_0\left|H_0^2\right|\beta_0 h}{2k_0}\left[\frac{1 + \mathrm{sinc}(2p_s h)}{\epsilon_r} + \frac{\cos^2(p_s h)}{\alpha_0 h}\right]. \quad (8)$$

B. Perturbed SW Propagation and Radiation Characteristics

The change in the propagation constant of the incident SW mode can now be obtained

$$\Delta\gamma \equiv \alpha + j\Delta\beta = \frac{P_{\rm Rad}/l}{2P_{\rm SW}} \quad (9)$$

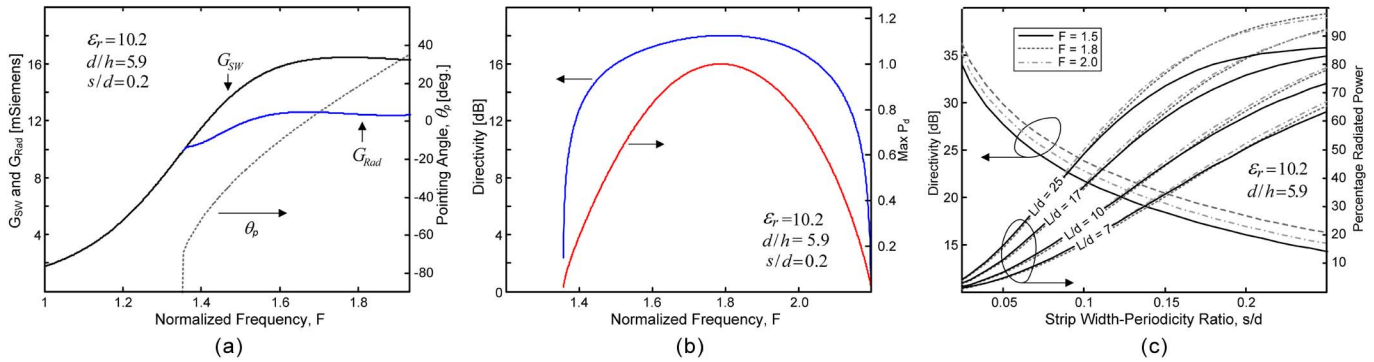

Fig. 3. (a) SW and radiation conductances, beam direction versus frequency F. (b) Beam directivity and peak power density versus F. (c) Calculated directivity [using Eq. (14)] versus the strip-width–periodicity ratio for $F = 1.5$, 1.8, and 2.0. Radiated powers are also shown for different antenna lengths.

as the rate of change of the SW power along the aperture $(dP_{\rm SW}/dz)$ can be equated to the radiated power, mainly

$$\frac{dP_{\rm SW}}{dz} = -2\Delta\gamma P_{\rm SW} = -P_{\rm Rad}/l \tag{10}$$

and since the perturbed SW power can be described by $P_0 e^{-2\Delta\gamma z}$ (where P_0 is defined as the unperturbed SW power at the origin). $\Delta\gamma$ is obtained by using (7) and (8) in (9). In addition, the factor α can describe the attenuation constant of the excited LW modes as dielectric losses are neglected. Thus, the complex wavenumber describing LW propagation along the aperture can now be defined

$$k_z^{\rm LW} = \beta_n + \Delta\beta - j\alpha. \tag{11}$$

As stated earlier, LW radiation can occur only from spatial modes with $n < 0$ since $\beta_0 > k_0$. The $n = -1$ harmonic is a spatial mode that can radiate whenever $-k_0 < \beta_{-1} + \Delta\beta < k_0$, which requires that

$$\frac{2\pi}{\beta_0 + \Delta\beta + k_0} < d < \frac{2\pi}{\beta_0 + \Delta\beta - k_0}. \tag{12}$$

The maximum radiated field is directed at an angle θ_p away from broadside ($+\hat{x}$-direction) and can be approximated by

$$\theta_p \approx \sin^{-1}\left(\frac{\beta_{-1} + \Delta\beta}{k_0}\right) = \sin^{-1}\left(\frac{\beta_0 + \Delta\beta - 2\pi/d}{k_0}\right). \tag{13}$$

Furthermore, the beam directivity is inversely proportional to the attenuation factor for a unidirectional LW and is given by

$$\text{Directivity } D = \frac{\sqrt{k_0^2 - (\beta_{-1} + \Delta\beta)^2}}{\alpha} \tag{14}$$

while the power radiation pattern R is a function of beam angle "θ" and is dependent on $k_z^{\rm LW}$, which defines the generated far-field pattern for an infinitely long 1-D LWA structure [9]

$$R(\theta) = \frac{\cos^2\theta}{\left|\sin\theta - k_z^{\rm LW}/k_0\right|^2}. \tag{15}$$

III. Results

To verify the above analysis, we consider the following parameters: $\epsilon_{\rm r} = 10.2$, $d/h = 5.9$ (= 7.49 mm/1.27 mm), $n = -1$, and $L/d = 14$, where L is the total length of the LWA structure. We shall assume that the metallic grating has a strip-width–periodicity ratio (s/d) of 0.2. The residual SW power left at $z = L$ after going through the leaky section is assumed to be absorbed with no reflection. This means that the total radiated power is related to the incident SW power by: $P_{\rm T,Rad} = P_{\rm SW}(1 - e^{-2\alpha L})$. The SW power is assumed to be launched by a slot excited by a voltage V_s, and reflector slots are assumed to act as parasitic elements that direct all the launched power in the forward $+\hat{z}$-direction. This launched SW power, $P_{\rm SW}$, has been derived in [8] and plotted versus F in Fig. 3(a) as the SW conductance $(= 2P_{\rm SW}/V_s^2)$ in milli-Siemens, with $V_s = 1$. The launched power has a peak around $F = 1.79$, and radiation starts to occur due to the $n = -1$ spatial harmonic at $F = 1.35$ with a backward beam at endfire. As frequency increases, the main beam position "θ_p" is scanned toward forward-fire. The beam directivity is also plotted versus F in Fig. 3(b), and it shows a broad maximum between $F = 1.5$ and 2.0. The peak power density $P_{\rm d}$ is proportional to the total radiated power $P_{\rm T,Rad}$ times the directivity. Relative values of $P_{\rm d}$ are also plotted, and it can be observed that there exists a maximum for $P_{\rm d}$ around $F = 1.8$, similar to the SW power.

An expression can be defined relating the percentage of radiated power or radiation efficiency, η, to the frequency of operation, antenna length, and LW attenuation constant, α, namely $\eta = 100(1 - e^{-2\alpha L})$. Calculations suggest that for a fixed d, power can leak away faster from the structure for a wider strip due to the increased perturbation of the incident $\rm TM_0$ SW mode. For example, for a strip-width-grating ratio of $s/d = 0.25$, an antenna length of 15 periods is required to radiate 90% of the input SW power at $F = 1.8$. Conversely, for $s/d = 0.15$, 21 periods is required to radiate at least 70% of the input power at the same frequency. The directivity [(14)] and radiated power are also compared in Fig. 3(c) and plotted versus s/d. It is seen that as s/d is reduced, the directivity increases, but the radiated power decreases. Calculated LW phase and attenuation constants (Fig. 4) are also compared to HFSS full-wave simulations of a finite LWA $(L/d = 14)$. General agreement can be observed for the infinite case and the finite structure suggesting respectable predictions for $k_z^{\rm LW}$.

Calculated power patterns $R(\theta)$ at different frequencies are shown in Fig. 5 using (15) for the ideal and infinitely long structure; i.e., $L/d \to \infty$. It is seen that the radiation is also optimized at $F = 1.8$ or $f = 22.3$ GHz. These results suggest that

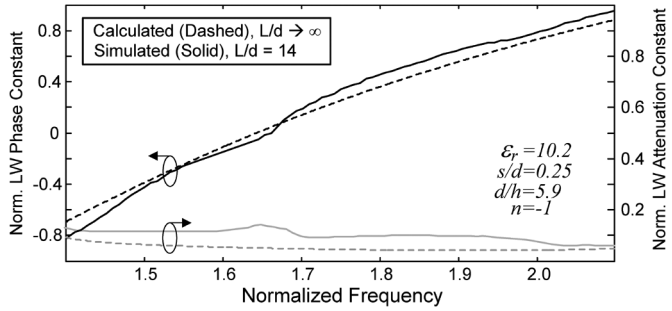

Fig. 4. LW phase and attenuation constants, respectively defined by $\mathrm{Re}\{k_z^{\mathrm{LW}}\} = \beta_n + \Delta\beta$ and $-\mathrm{Im}\{k_z^{\mathrm{LW}}\} = \alpha$ and normalized by k_0.

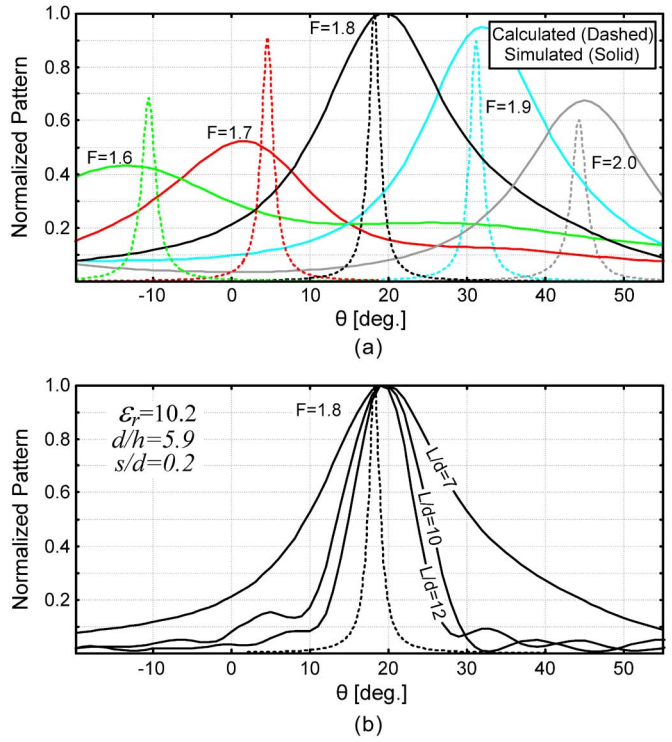

Fig. 5. Radiation patterns at five frequencies are shown in (a): $F = 1.6$ (19.8 GHz), 1.7 (21.1 GHz), 1.8 (22.3 GHz), 1.9 (23.5 GHz), and 2.0 (24.8 GHz). Values are normalized to the observed maximum at $F = 1.8$. By comparing the simulated beam patterns, as L/d increases in (b), better agreement can be observed with the calculated pattern ($L/d \rightarrow \infty$). This implies respectable calculations for α.

for optimum radiation performances, SW power levels should be maximized; i.e., slot excitation and LWA operation should be near a SW power peak. Numerical results are also compared to HFSS simulations of a linear 1-D LWA [with $L/d = 7$ in Fig. 5(a)]. A short structure with only seven periods was simulated to illustrate the effect of antenna length on the radiated field [similar to the analysis in Fig. 3(c)]. It should be noted that the simulated beamwidths will also decrease for a longer antenna aperture ($L/d > 7$) with improved beam directivity, and thus a better agreement with the calculated pattern can be observed [Fig. 5(b)]. In addition, agreement is shown in Fig. 5(a) for the main beam positions and the region for maximum radiated power ($F = 1.8$).

Fig. 6 compares calculated pointing angles to recent measurements and HFSS simulations of two LWA structures fed by

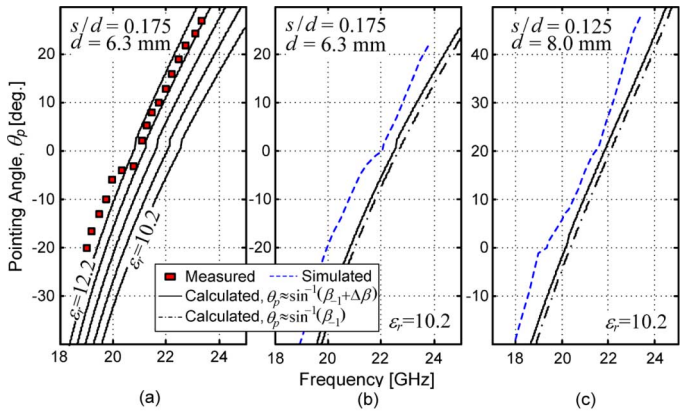

Fig. 6. Comparison of pointing angles for various LWA structures versus frequency: $s/d = 0.175$ in (a) and (b), and $s/d = 0.125$ in (c). An example of the examined planar antenna is shown in Fig. 2.

SWLs [5], [6] as in Fig. 2. General agreement can be observed for the estimations using (13). Deviations in θ_p are a likely result of substrate variations and fabrication tolerances. It should be noted that similar downward frequency shifts between measurements and simulations were previously reported by the authors for other dielectric-based LWA designs fed by SWs [6]. To further investigate these effects, a parametric analysis was completed by calculating θ_p for varied ϵ_{r} as shown in Fig. 6(a). By increasing the relative dielectric constant of the utilized GDS to 12.2 in increments of 0.5 from the rated 10.2 (at 10 GHz) by Rogers Corporation, while maintaining all other parameters, a better agreement in the measurements and calculations is observed. Results suggest that for this LWA structure, the dielectric constant was approximately 12. Such practical effects may be expected when operating at microwave and millimeter-wave frequencies.

Ideally, the strip width should be small relative to the periodicity ($s/d \ll 1$) and guided wavelength, $\lambda_{\mathrm{SW}} (= 2\pi/\beta_0)$. For instance, to achieve leakage of the $n = -1$ spatial harmonic, grating periodicity should be of the same order as λ_{SW} [by (12)]. Suitable s/d ratios are investigated in this letter ($d = 6.3$, 7.49, and 8.0 mm, $\lambda_{\mathrm{SW}} = 7.5$ mm at 20 GHz) and are typical of such SW-fed LWA structures [5], [6]. Effectively, the $s/d \ll 1$ requirement is comparable to $s/\lambda_{\mathrm{SW}} \ll 1$, and it can be observed that the accuracy of the calculations increases as s/d is reduced. For example, in Fig. 6(b) for $s/d = 0.175$, θ_p is equal to 20° at 23.6 and 24.4 GHz for the simulations and calculations, respectively. A difference of 0.8 GHz can be observed. Increased accuracy is obtained for the predicted values based on (13) as can be seen in Fig. 6(c); differences in the calculations and simulations are reduced to only 0.4 GHz at $\theta_p = 20°$. These results are expected since the purposed analysis assumes $s/d \ll 1$, meaning that the presented approach is suitable for gratings widths that are ≈25% (or less) of d. Improved accuracy may be possible for narrower strip LWAs.

It should also be mentioned that these calculated values offer better predictions when compared to the classic pointing angle approximation [9]: $\theta_p \approx \sin^{-1}(\beta_{-1}/k_0)$, (13), just with no perturbation term $\Delta\beta$. For instance, in Fig. 6(c) at 21.4 [21.8] ⟨22.0⟩ GHz, $\theta_p = 20°$ for the simulations [the calculations

using (13)] $\langle \theta_p \approx \sin^{-1}(\beta_{-1}/k_0) \rangle$. Dielectric losses were also included in the structure modeling $(\tan\delta = 0.0023)$ and for the calculations using (13). In addition, a reactive power loss factor was added to (7) to account for strip conductor losses ($P_{\mathrm{Rad}}/l' = P_{\mathrm{Rad}}/l - jexp\{-2\ s\ \alpha_c/d\}P_{\mathrm{Rad}}/l$, with $\alpha_c = 0.0001$). For near-broadside radiating frequencies ($\theta_p \approx 0^\circ$), scanning is not continuous and suggests LW stopband behavior; this scanning behavior is typically observed for such one-sided LWA structures [6]. Improved accuracy in the predictions may also be possible if the presented analysis is extended to radial SW and LW fields and finite strips.

IV. Conclusion

An accurate but simple perturbation analysis of SW-driven LWAs was presented. By examining the transition from a SW to a LW guiding section, the attenuation and phase constants can be determined along with the beam directivity, efficiency, and radiated power relative to the incident SW power. The analysis can also be extended to other LW-based structures.

References

[1] T. Zhao, D. R. Jackson, J. T. Williams, H. Y. D. Yang, and A. A. Oliner, "2D periodic leaky wave antennas-part I: Metal patch design," *IEEE Trans. Antennas Propag.*, vol. 53, no. 11, pp. 3505–3514, Nov. 2005.

[2] P. Burghignoli, G. Lovat, and D. R. Jackson, "Analysis and optimization of leaky-wave radiation at broadside from a class of 1-D periodic structures," *IEEE Trans. Antennas Propag.*, vol. 54, no. 9, pp. 2593–2604, Sep. 2006.

[3] P. Baccarelli, P. Burghignoli, F. Frezza, A. Galli, P. Lampariello, G. Lovat, and S. Paulotto, "Modal properties of surface and leaky waves propagating at arbitrary angles along a metal strip grating on a grounded slab," *IEEE Trans. Antennas Propag.*, vol. 53, no. 1, pp. 36–46, Jan. 2005.

[4] M. Ettorre, S. Bruni, G. Gerini, A. Neto, N. Llombart, and S. Maci, "Sector PCS-EBG antenna for low-cost high-directivity applications," *IEEE Antennas Wireless Propag. Lett.*, vol. 6, pp. 537–539, 2007.

[5] S. K. Podilchak, "Planar leaky-wave antenna designs for directive beam scanning," M.Sc. thesis, Dept. Elect. Comput. Eng., The Royal Military College and Queen's University, Kingston, ON, Canada, 2008.

[6] S. K. Podilchak, A. P. Freundorfer, and Y. M. M. Antar, "Planar leaky-wave antenna designs offering conical-sector beam scanning and broadside radiation using surface-wave launchers," *IEEE Antennas Wireless Propag. Lett.*, vol. 7, pp. 155–158, 2009.

[7] H. Hammad, Y. M. M. Antar, A. Freundorfer, and S. Mahmoud, "Uniplanar CPW-fed slot launchers for efficient TM0 surface wave excitation," *IEEE Trans. Microw. Theory Tech.*, vol. 51, no. 4, pp. 1234–1240, Apr. 2003.

[8] S. Mahmoud, Y. Antar, H. Hammad, and A. Freundorfer, "Theoretical considerations in the optimization of surface waves on a planar structure," *IEEE Trans. Antennas Propag.*, vol. 52, no. 8, pp. 2057–2063, Aug. 2004.

[9] T. Tamir, *Antenna Theory, Part 2*, R. E. Collin and F. J. Zucker, Eds. New York: McGraw-Hill, 1969, ch. 20.